Sustained hyperglycemia specifically targets translation of mRNAs for insulin secretion

Abigael Cheruiyot, Jennifer Hollister-Lock, Brooke Sullivan, Hui Pan, Jonathan M. Dreyfuss, Susan Bonner-Weir, and Jean E. Schaffer

Joslin Diabetes Center, Harvard Medical School, Boston, Massachusetts, USA.

Pancreatic β cells are specialized for coupling glucose metabolism to insulin peptide production and secretion. Acute glucose exposure robustly and coordinately increases translation of proinsulin and proteins required for secretion of mature insulin peptide. By contrast, chronically elevated glucose levels that occur during diabetes impair β cell insulin secretion and have been shown experimentally to suppress insulin translation. Whether translation of other genes critical for insulin secretion is similarly downregulated by chronic high glucose is unknown. Here, we used high-throughput ribosome profiling and nascent proteomics in MIN6 insulinoma cells to elucidate the genome-wide impact of sustained high glucose on β cell mRNA translation. Before induction of ER stress or suppression of global translation, sustained high glucose suppressed glucose-stimulated insulin secretion and downregulated translation of not only insulin, but also mRNAs related to insulin secretory granule formation, exocytosis, and metabolism-coupled insulin secretion. Translation of these mRNAs was also downregulated in primary rat and human islets following ex vivo incubation with sustained high glucose and in an in vivo model of chronic mild hyperglycemia. Furthermore, translational downregulation decreased cellular abundance of these proteins. Our study uncovered a translational regulatory circuit during β cell glucose toxicity that impairs expression of proteins with critical roles in β cell function.

Introduction

Diabetes results from failure of pancreatic β cells to secrete sufficient insulin to regulate glucose homeostasis. Progressive decline in β cell function occurs in the setting of hyperglycemia during the progression from early appearance of autoantibodies to frank type 1 diabetes, and during the evolution from compensated insulin resistance to type 2 diabetes (1, 2). In type 1 diabetes, intensive insulin therapy that restores normal glycemic levels increases stimulated C-peptide levels, a reflection of improved insulin biosynthesis and preserved β cell function (3). In patients with newly diagnosed type 2 diabetes, intensive short-term insulin therapy improves β cell function and long-term glycemic control (4, 5). These observations support the hypothesis that glucose toxicity contributes to decline in insulin production in diabetes.

β Cells are specialized to couple glucose metabolism not only to insulin secretion, but also to robust insulin peptide production. In response to an acute physiological rise in glucose, proinsulin mRNA translation rapidly increases within 30–60 minutes, without change in insulin mRNA abundance (6). This translational regulation requires sequences predicted to form a stem-loop structure within the 5′-untranslated region (5′-UTR) of the insulin mRNA that bind to protein factors in a glucose-dependent fashion (7). In addition to insulin, glucose acutely upregulates translation of pro-

teins involved in glucose metabolism, insulin processing, secretory granule biogenesis, and insulin exocytosis, without causing an equivalent increase in total protein synthesis (8–11). Given that newly synthesized insulin is preferentially released initially, this mRNA translational program supports physiological increases in glucose-stimulated insulin secretion (GSIS) following brief exposures to high glucose (12).

By contrast, persistently elevated glucose impairs GSIS and insulin translation. Among obese subjects, GSIS decreases with increasing plasma glucose area under the curve in a 3-hour oral glucose tolerance test, without change in insulin sensitivity (13). Ex vivo incubation of isolated human or rodent islets over 1 week in medium containing high glucose also impairs GSIS and inhibits translation of proinsulin (14, 15). The impact of sustained high glucose on GSIS in cadaveric human islets is apparent as early as 2 days after exposure to high glucose, a time point at which impairment is reversible, associated with only modest transcriptomic changes, and without evidence for ER stress (16). Sustained exposure of insulinoma cells and isolated islets to high concentrations of glucose and saturated fatty acids to model the metabolic stress of type 2 diabetes increases translation of JUND, a transcriptional regulator of β cell apoptosis, and induces ER stress (17, 18). However, it is not known whether sustained high glucose alone initiates programmatic regulation of translation prior to induction of ER stress.

Given the importance of translational regulation in GSIS, we sought to gain insight into the impact of sustained glucose elevation on genome-wide β cell mRNA translation. Using complementary high-throughput approaches in a MIN6 model and validating our findings in primary isolated islets ex vivo and in an in vivo model of hyperglycemia, we show that chronic glucose excess

coordinately downregulates translation of genes that function in metabolism-coupled insulin secretion.

Results

Sustained high glucose impairs insulin translation independent of ER stress. Exposure of primary isolated human or rat islets to high glucose for 1 week increases basal secretion and impairs GSIS in human and rodent islets (14, 15, 19). We cultured hand-picked isolated primary rat islets in medium containing 16.7 mM glucose versus 5.5 mM glucose. Islets were then rested in medium with 2.8 mM glucose for 1 hour before assaying for GSIS (Figure 1A). Compared with low glucose, islets incubated in high glucose for only 4 days had increased basal insulin secretion (Figure 1B). Although the amount of insulin secreted following stimulation increased in islets exposed to sustained high glucose, the stimulation index was decreased by 69% (Figure 1B), without impact on total islet insulin content (Figure 1C). Shorter incubations in high glucose did not decrease GSIS (not shown). Exposure to high glucose over 4 days did not cause dedifferentiation or transdifferentiation, as expression of β cell identity genes was similar between the 2 glucose conditions (Figure 1D). Although global protein synthesis was unchanged between the glucose conditions (Figure 1E), sustained high glucose decreased the rate of insulin synthesis (Figure 1F). Pancreatic β cells are particularly susceptible to increased ER stress, and prolonged ER stress is detrimental to β cell function (20, 21). However, treatment with high glucose over 4 days did not increase the phosphorylation of PERK or expression of ATF4, well-established upstream regulators of ER stress (Figure 1G). Thus, 4 days of exposure to sustained high glucose decreased translation of insulin before suppression of global protein synthesis, compromised β cell identity, or sustained engagement of the unfolded protein response pathway.

MIN6 cells model chronic high glucose effects on islet insulin translation. Pancreatic islets are micro-organs that consist of several cell types, including glucagon-containing α cells, somatostatin-containing δ cells, and polypeptide-producing PP cells, in addition to insulin-producing β cells. To delineate the effects of chronic high glucose specifically on β cells and to identify a system that more readily provides sufficient material for high-throughput analyses, we modeled chronic high glucose exposure in early-passage MIN6 insulinoma cells that support robust GSIS (22). These cells are typically propagated in 25 mM glucose to sustain rapid cell growth but can be maintained for limited periods in lower glucose with slower growth. Following incubation for 24 hours in 5.5 mM glucose, stimulatory glucose caused a 10-fold increase in insulin secretion (Figure 2, A and B). Basal insulin secretion did not increase in MIN6 cells maintained in high glucose, contrary to observations in islets. However, similarly to observations in islets, the stimulation index was decreased by 59% by high glucose (Figure 2B). Although high glucose decreased insulin content of MIN6 cells, the impact of sustained high glucose on GSIS remained significant even when secretion was calculated as a percentage of insulin content (Figure 2, C and D). This did not reflect a general response to increased osmolarity, since incubation in low-glucose medium supplemented with mannitol did not decrease GSIS (Figure 2E). As observed in rat islets, β cell identity markers were similar in both glucose conditions, and sustained high glucose specifically decreased insulin

translation without affecting global protein synthesis or inducing ER stress (Figure 2, F–I). Taken together, these results demonstrate that 24-hour treatment of MIN6 cells with 25 mM glucose versus 5.5 mM glucose models the effects of sustained high glucose on GSIS and insulin mRNA translation in primary islets.

Ribosome profiling identifies broad impact of sustained high glucose on gene-specific mRNA translation. Incubation of MIN6 cells or islets in high-glucose medium supplemented with high concentrations of the saturated fatty acid palmitate induces ER stress and has profound effects on mRNA translation (17, 18). To determine the genome-wide effects of sustained high glucose alone on β cell mRNA translation in the absence of ER stress, we compared the translatome of MIN6 cells in low versus high glucose by ribosome profiling. This RNA sequencing method is based on the principle that more efficiently translated mRNAs are associated with more ribosomes and therefore generate more ribosome-protected footprints (RPFs) upon nuclease digestion. Both RPF and total RNA libraries were sequenced from cells following treatment for 24 hours with 25 mM versus 5.5 mM glucose (Figure 3A). As observed in other ribosome profiling studies of mammalian cells (23), peak RPF fragment sizes were 30–35 bp, RPFs were enriched for open reading frames of genes compared with mRNAs, and RPF sequences showed triplet periodicity (Figure 3, B–D).

Sustained high glucose had substantial impact on the transcriptome (Figure 3E and Supplemental Table 1 [supplemental material available online with this article; https://doi.org/10.1172/JCI173280DS1] for 7,117 genes that met FDR < 0.01), consistent with prior studies (16). We observed greater representation of 3′-UTR reads in the transcriptome under high glucose conditions (Figure 3C), suggesting that transcriptionally upregulated genes may have longer 3′-UTR sequences. There were also many changes in the translatome that met FDR < 0.1 (Figure 3F and Supplemental Table 2 for 2,728 genes that met FDR < 0.1). To identify genes for which glucose treatment specifically altered mRNA translation regulation, we calculated translation efficiency (TE) as the ratio of normalized RPF reads to normalized total mRNA reads per gene (Figure 3G). This measure accounts for changes in transcription and enables identification of genes for which changes in translation do not simply parallel changes in mRNA abundance. Using FDR < 0.1, we found that sustained high glucose upregulated the TE of 3,393 genes and downregulated the TE of 3,382 genes (Supplemental Table 3). Among genes for which TE was upregulated by chronic high glucose, pathways related to chromatin organization, RNA splicing, translation, deubiquitination, and M phase of the cell cycle were overrepresented (Figure 3H). Among genes for which TE was downregulated by chronic high glucose, pathways important for β cell function including insulin processing, ER-to-Golgi transport, glucose metabolism, and TCA cycle were overrepresented (Figure 3I). Thus, independent of ER stress or change in global protein synthesis rates, sustained high glucose had genome-wide effects on translation. Moreover, in addition to insulin, sustained high glucose downregulated translation of other genes required for metabolism-coupled insulin secretion.

Nascent proteomics as an independent measure of glucose-altered translation. Our ribosome profiling analysis in MIN6 cells identified a large number of genes for which translation was affected by sustained high glucose based on the ratio of RPFs to
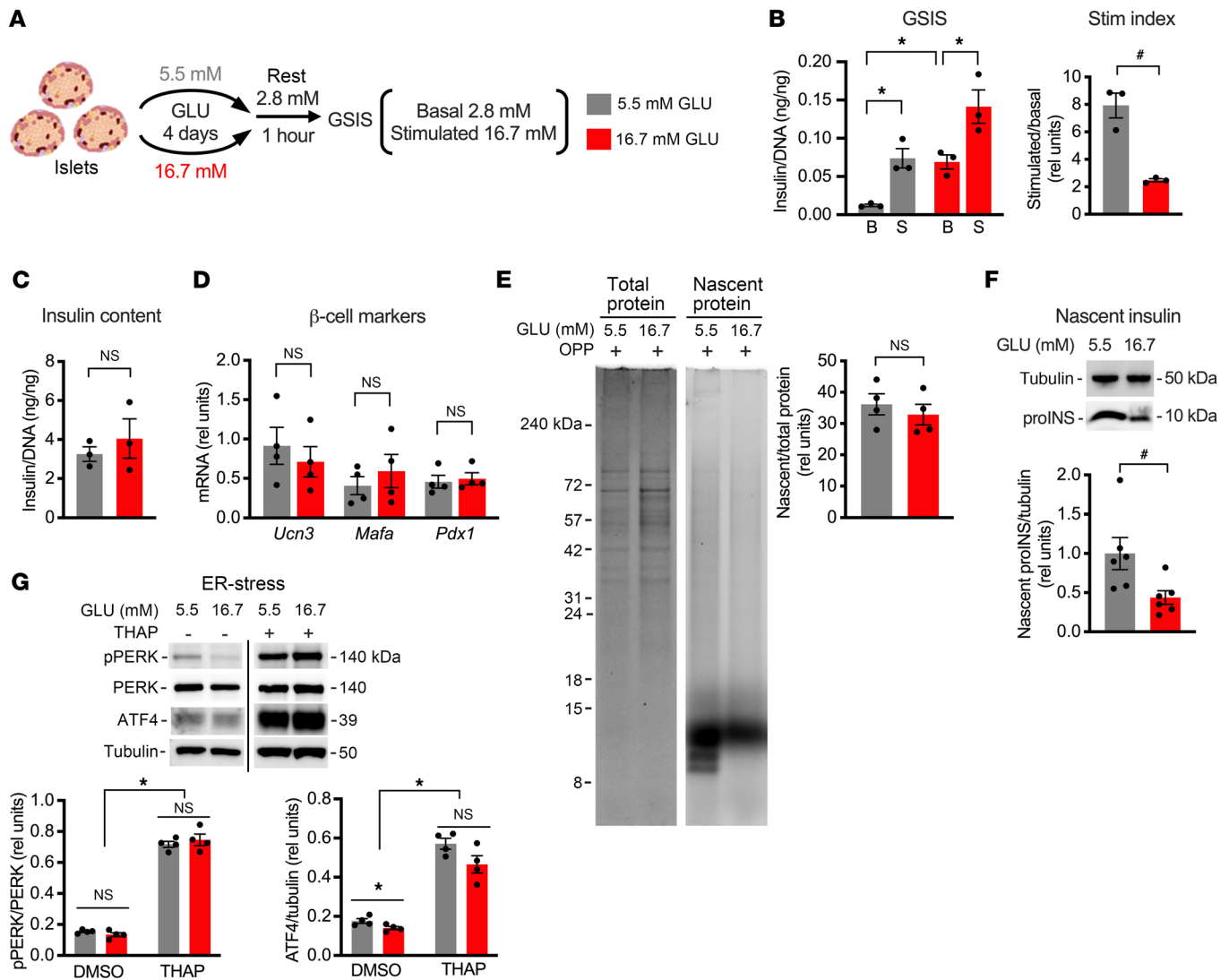
Figure 1. Sustained high glucose decreases basal insulin translation in isolated rat islets. Hand-picked islets from adult Sprague-Dawley rats were cultured for 4 days in medium containing 5.5 mM (gray) or 16.7 mM (red) glucose (GLU). (**A**) One hour of resting in 2.8 mM GLU was followed by GSIS quantified at 2.8 mM (basal, B) and 16.7 mM (stimulated, S) GLU. (**B**) GSIS normalized by DNA with stimulation (Stim) index quantified as stimulatory/basal secretion. (**C**) Insulin content normalized to DNA. (**D**) Quantification of β cell markers *Ucn3*, *Mafa*, and *Pdx1* relative to 18S rRNA by quantitative PCR (qPCR). (**E**) Cells were pulse-labeled with *O*-propargyl-puromycin (OPP) and analyzed by SDS-PAGE. Total protein was quantified by Coomassie stain (left), and newly synthesized protein was quantified by click-addition of Alexa Fluor 647 (right). Representative images with quantification. (**F**) Metabolic labeling with OPP was followed by click-biotin addition and streptavidin pull-down of nascent proteins. Immunoblot analysis of newly synthesized proinsulin (proINS) with tubulin control. (**G**) Representative immunoblots and quantification for ER stress markers with thapsigargin-treated (THAP-treated) control. Mean ± SEM for n = 3–4 independent experiments. *Adjusted P value (P_{adj}) < 0.05, 2-way ANOVA with Bonferroni's post hoc correction (**B** [GSIS], **D**, and **G**). #P < 0.05, unpaired t test (**B** [Stim index], **C**, and **E**) or ratio-paired t test (**F**).

total mRNA. To corroborate and filter these results, we used an orthogonal method of translation analysis in which nascent peptides were pulse-labeled with the methionine analog azidohomoalanine (AHA), click-biotin-conjugated, enriched by streptavidin pull down, and analyzed by mass spectrometry–based proteomics (Figure 4A). (Figure 4A). Principal component analysis revealed distinct patterns of nascent protein synthesis under the different glucose treatment conditions (Figure 4B). Sustained high glucose significantly affected new peptide synthesis for many genes (Figure 4C), and this correlated well with abundance of RPF sequences in ribosome profiling (Figure 4D).

To identify high-confidence glucose-driven translation changes, we examined the overlap between nascent proteomics and ribosome profiling TE, focusing on proteins for which changes in both analyses met FDR < 0.1 and 20% log$_2$ fold change. Based on these criteria, 207 proteins were upregulated by sustained high glucose (Figure 4E and Supplemental Table 4). However, this group did not contain "disallowed" genes, whose upregulation is known to lead to impaired insulin secretion (24). On the other hand, proteins known to function in insulin production and GSIS were found among the 183 downregulated proteins (Figure 4F and Supplemental Table 4). Given that sustained high glucose downregulates GSIS and insulin
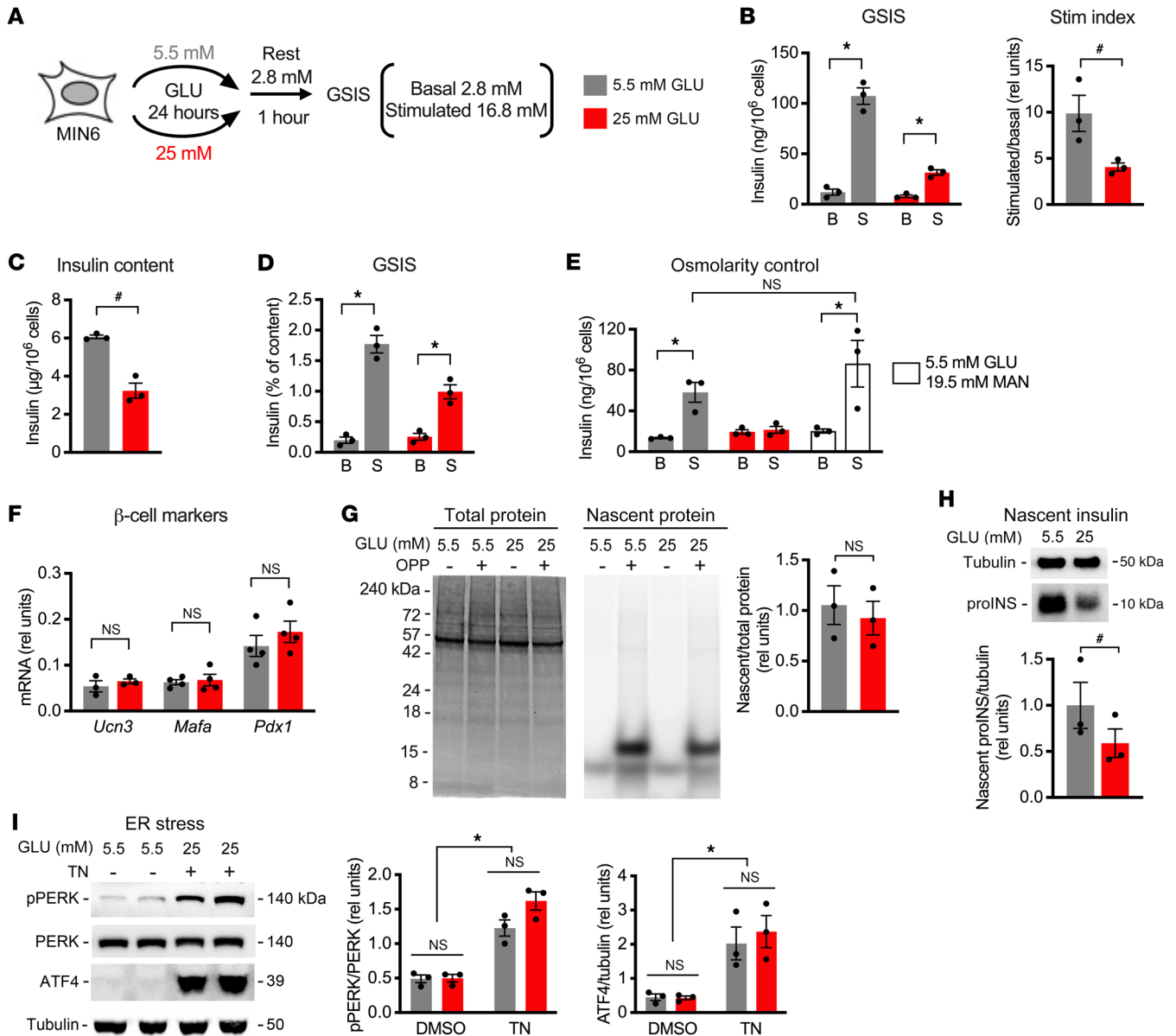
Figure 2. Sustained high glucose decreases insulin synthesis in MIN6 cells. MIN6 cells were incubated in medium containing 5.5 mM (gray) or 25 mM (red) GLU for 24 hours. (**A**) One hour of resting in 2.8 mM GLU was followed by GSIS quantified at 2.8 mM (B) and 16.8 mM (S) GLU. (**B**) GSIS normalized by cell number with stimulation index quantified as stimulatory/basal secretion. (**C**) Insulin content per 10^6 cells. (**D**) GSIS normalized to cellular insulin content. (**E**) GSIS normalized by cell number following incubation in 5.5 mM GLU, 25 mM GLU, or 5.5 mM GLU with 19.5 mM mannitol (MAN, open bars). (**F**) qPCR quantification of β cell markers *Ucn3*, *Mafa*, and *Pdx1* relative to 18S rRNA. (**G**) OPP pulse labeling and SDS-PAGE. Total protein was quantified by Coomassie stain, and newly synthesized protein was quantified by click-addition of Alexa Fluor 647. Representative images with quantification. (**H**) OPP labeling, click-biotin addition, and streptavidin pull-down of nascent proteins. Immunoblot for newly synthesized proINS and tubulin control. (**I**) Representative immunoblots and quantification for ER stress markers with tunicamycin-treated (TN-treated) control. Mean ± SEM for n = 3–4 independent experiments. *P_{adj} < 0.05, 2-way ANOVA with Bonferroni's post hoc correction (**B** [GSIS], **D**, **E**, and **I**). #P < 0.05, unpaired t test (**B** [Stim index], **C**, and **G**) or ratio-paired t test (**H**).

translation, we focused on downregulated proteins known to function in insulin production and metabolism-coupled insulin secretion (Table 1). As expected, translations of mRNAs for INS were downregulated. Among the other translationally downregulated proteins, SCGN (secretagogin) is an EF-hand Ca²⁺-binding protein that regulates F-actin dynamics, focal adhesion remodeling, and second-phase insulin secretion in β cells, and its knockdown impairs GSIS (25–27). VPS41, a component of the homotypic func-

tion and vacuole protein sorting complex, and SLC30A8, which transports zinc into insulin granules, are both required for optimal GSIS (28, 29). SLC2A2, the plasma membrane glucose transporter in rodent β cells, and IDH2, which functions in reductive flux of glutamine to citrate in the mitochondria, are critical for metabolism-coupled insulin secretion (30–32). While PFKFB3 and IGF2 were not detected in our nascent proteomics, they were significantly downregulated by high glucose in ribosome profiling and were
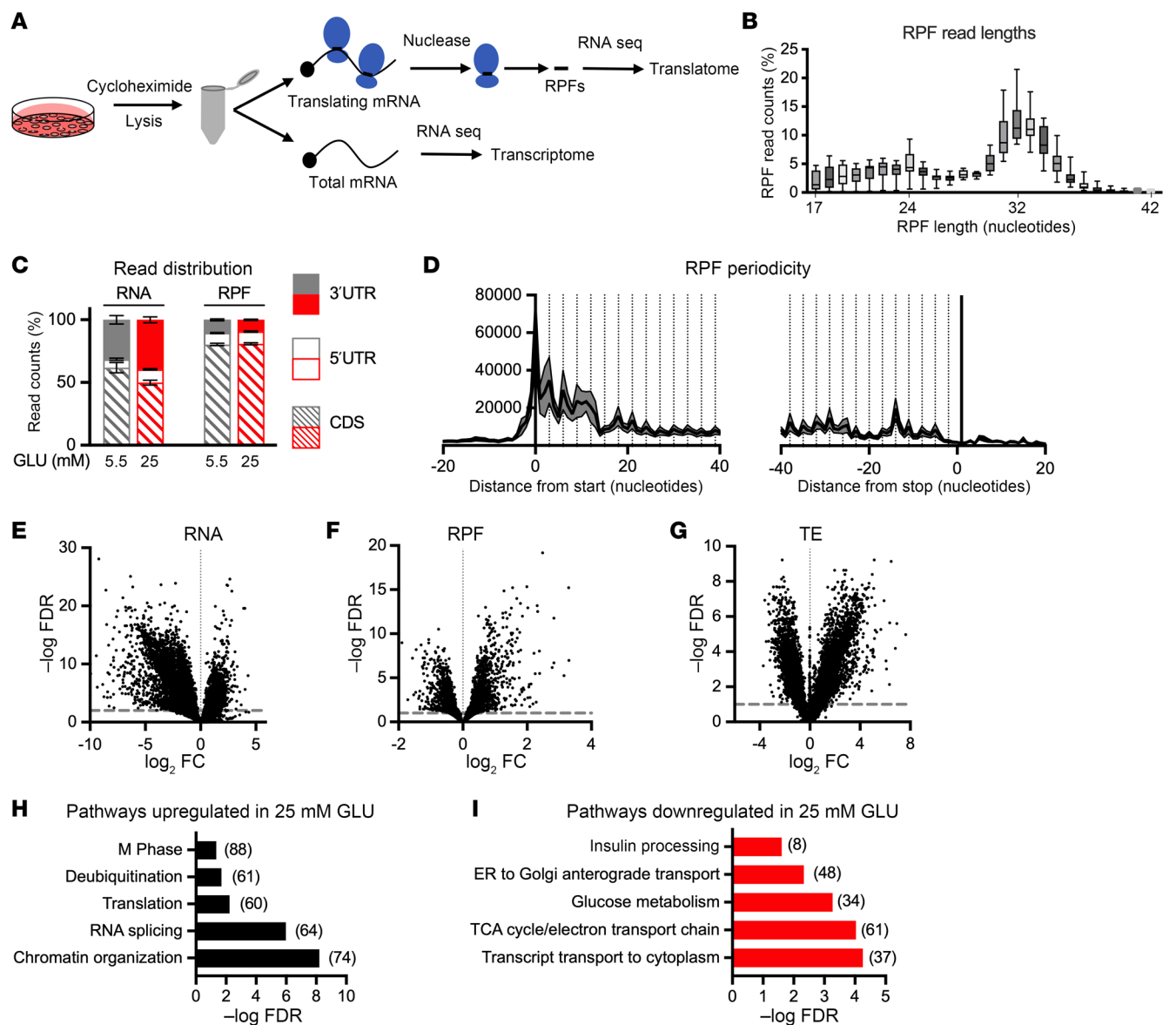
Figure 3. Sustained high glucose treatment has genome-wide impact on translation. MIN6 cells incubated in medium containing 5.5 mM (gray) or 25 mM (red) GLU for 24 hours were analyzed by ribosome profiling. (**A**) Workflow for RNA sequence analysis of ribosome-protected footprints (RPFs; translatome) and total RNA (transcriptome). (**B**) RPF read lengths. Boxes indicate 25th to 75th percentiles, line in middle of box is the median, and whiskers go from smallest to largest values. (**C**) Distribution of reads to coding sequence (CDS; hatched), 5′-UTR (open), and 3′-UTR (filled) for RNAs and RPFs. (**D**) Triplet periodicity of RPFs near CDS start and stop. (**E**–**G**) Volcano plots of –log FDR versus log$_2$ fold change (FC), calculated for 25 mM versus 5.5 mM GLU for RNA (**E**; dotted line FDR = 0.01), RPF (**F**; dotted line FDR = 0.1), and translation efficiency (TE = RPF/RNA; **G**; dotted line FDR = 0.1). (**H** and **I**) Representative Reactome gene sets overrepresented at a significance threshold FDR < 0.05 as upregulated (**H**) and downregulated (**I**) by 25 versus 5.5 mM glucose. Numbers of regulated genes in pathways indicated by numbers in parentheses. *n* = 8 independent samples per condition.

included in further analyses given established roles in potentiating insulin secretion (33, 34). Prior studies show that knockdown or knockout of each of these genes diminishes GSIS with more modest effect or no effect on basal secretion. In our ribosome profiling analysis, RPFs for these genes were similarly distributed over the 5′-untranslated and coding regions in high- and low-glucose samples, without evidence for new upstream open reading frames or pausing in sustained high glucose (Figure 4G, representative traces for SCGN and IDH2).

Validation of translational changes and impact on steady-state protein abundance. To confirm these chronic glucose-induced transla-

tion changes, we first quantified the ratio of mRNA associated with actively translating polysomes relative to total mRNA as a measure of TE in MIN6 cells incubated in 25 versus 5.5 mM glucose for 24 hours. Sustained high glucose decreased TE of *Ins1*, *Ins2*, *Scgn*, *Slc2a2*, *Pfkfb3*, *Slc30a8*, *Vps41*, *Idh2*, and *Igf2* (Figure 5A). *Actb* and *Tubg1* were unchanged by high glucose, consistent with lack of change in nascent protein. To determine whether changes in TE impacted protein levels, we quantified steady-state protein abundance in lysates of MIN6 cells treated with 25 versus 5.5 mM glucose. Sustained high glucose significantly decreased cellular content of SCGN, SLC2A2, PFKFB3, SLC30A8, VPS41, IDH2, and IGF2 (Figure 5B).
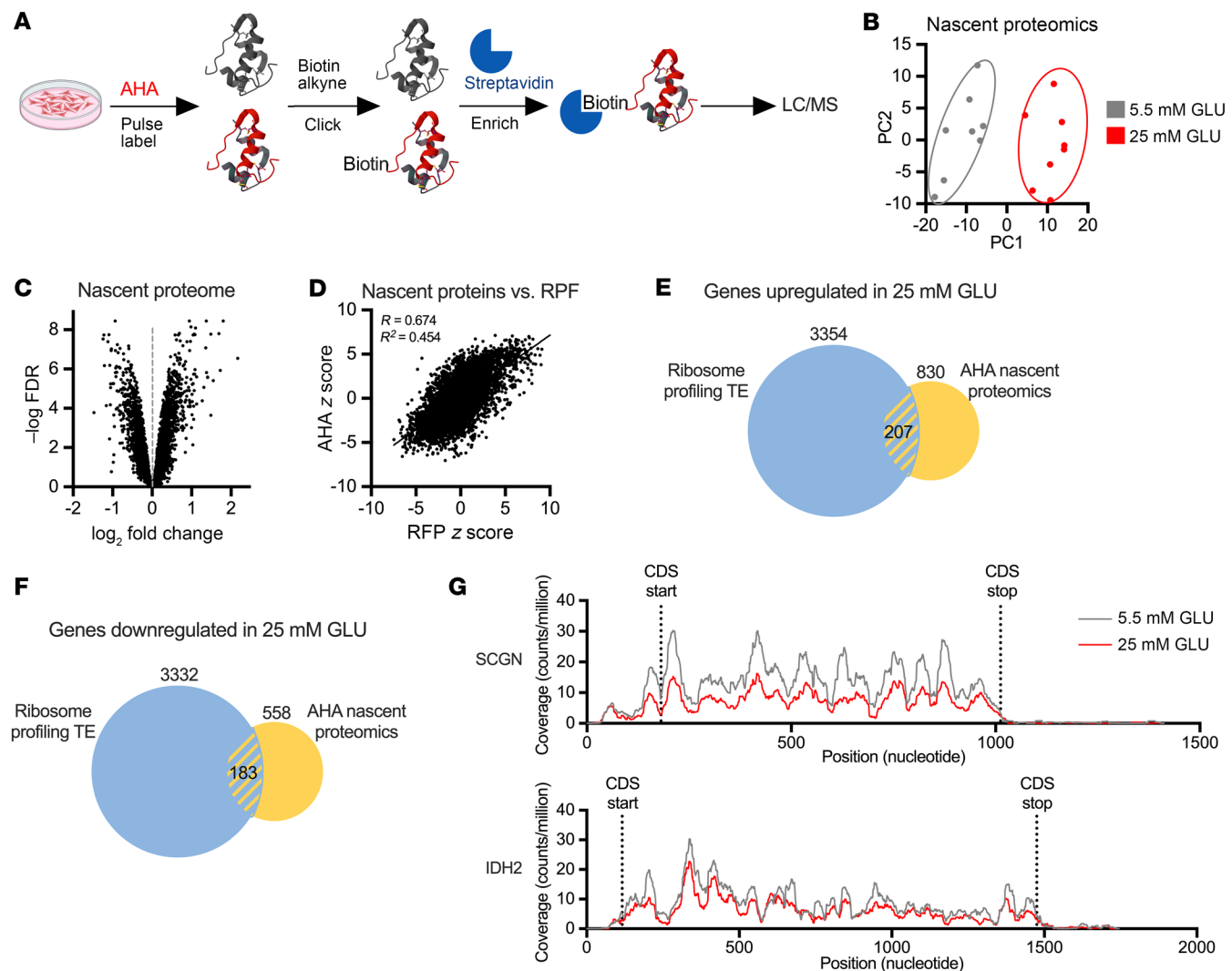
Figure 4. Sustained high glucose treatment has genome-wide impact on nascent proteome. MIN6 cells incubated for 24 hours in medium containing 5.5 mM (gray) or 25 mM (red) GLU were analyzed by nascent proteomics. (**A**) Workflow. (**B**) Surrogate variable principal component analysis. (**C**) Volcano plots of −log FDR versus $\log_2$ FC, calculated for 25 versus 5.5 mM GLU. (**D**) Correlation analysis of nascent proteomics z scores versus RPF z scores. (**E** and **F**) Overlap of proteins upregulated (**E**) or downregulated (**F**) by 25 mM versus 5 mM GLU in both TE and nascent proteomics data sets. −log FDR > 1 and $\log_2$ FC > 20%. (**G**) Representative RPF gene coverage plots for SCGN and IDH2, showing no evidence for new upstream open reading frames or pausing in 25 mM GLU. n = 8 independent samples per condition. CDS, coding sequence.

Although MIN6 cells were an important tool for technically challenging high-throughput discovery studies, these cells replicate rapidly, grow dispersed in cell culture, and lack the complex cellular makeup and architecture of islets. We next validated our findings in isolated rat islets using the conditions established above that impair glucose-stimulated insulin translation and secretion (Figure 1). Given the large amount of tissue needed to collect actively translating polysomes and limited number of islets, we quantified ribosome-associated (rather than polysome-associated) mRNA relative to total mRNA as a measure of TE. Sustained high glucose decreased TE for *Ins1, Ins2, Scgn, Slc2a2, Pfkfb3, Slc30a8, Vps41, Idh2,* and *Igf2*, without affecting TE of *Actb* and *Tubg1* (Figure 6A). As observed in MIN6 cells, this led to significantly decreased steady-state protein abundance for SCGN, SLC2A2, PFKFB3, VPS41, IDH2, and IGF2 and a trend for decrease in SLC30A8 that did not reach significance (Figure 6B). Collectively,

our results in primary islets and in MIN6 cells confirm findings from ribosome profiling and provide evidence that the translational regulation we uncovered has a meaningful impact on the β cell proteome.

To investigate the clinical relevance of the observed glucose effects on translation, we analyzed TE and protein abundance following incubation of cadaveric human islets in 20 versus 5.5 mM glucose (Figure 7A). Exposure of human islets to high glucose for 2 days caused a trend for increased basal insulin secretion (that did not reach statistical significance when secreted insulin was normalized to islet genomic DNA) and significantly decreased both GSIS and stimulation index (Figure 7B), consistent with previous reports (16). Insulin content of human islets incubated in high glucose trended down (Figure 7C), and the impact of sustained high glucose on basal insulin secretion was significant when normalized for insulin content (Figure 7D). TE, as assessed by ribosome-associated/total mRNA, was decreased for *INS, SCGN, PFKFB3,*

Table 1. Insulin synthesis/secretion genes translationally downregulated by sustained high glucose[A]

Gene symbol	Role	Ribosome profiling TE		Nascent proteomics	
		$\log_2$ FC	−log FDR	$\log_2$ FC	−log FDR
Idh2	Insulin secretion through reductive TCA flux	−1.99	3.61	−0.54	6.22
Igf2	Autocrine signaling promotes insulin secretion	−1.34	2.29	ND	ND
Ins1	Insulin gene	−0.77	1.14	−0.72	3.61
Ins2	Insulin gene	−1.45	2.29	[B]	[B]
Pfkfb3	Potentiates GSIS through regulation of glucokinase	−2.43	4.54	ND	ND
Scgn	Ca^{2+}- and insulin-binding protein that enhances GSIS	−0.99	1.79	−0.85	4.86
Slc2a2	Transports glucose for metabolism-coupled insulin secretion	−1.03	2.67	−0.45	1.44
Slc30a8	Transports Zn^{2+} into insulin secretory granules	−1.16	3.20	−0.36	2.90
Vps41	Endolysosomal protein in insulin secretory granule formation	−1.26	3.05	−0.41	4.05

[A]Sustained high glucose decreases translation efficiency and nascent peptides by 20% or more with FDR < 0.1. [B]Detection limited by peptide overlap with Ins1. ND, not detected.

and *VPS41* (Figure 7E). TE for *SLC30A8* trended down but did not reach statistical significance. TE for *IDH2* and *IGF2* was unchanged. Although translation of *SLC2A2* was unchanged, TE for *SLC2A1*, the main plasma membrane glucose transporter in human islets (35), was decreased. Consistent with findings in rodent islets, decreased TE led to decreased steady-state protein abundance for INS, SCGN, SLC2A1, PFKFB3, and SLC30A8 (Figure 7F).

To extend our findings to an in vivo model of hyperglycemia, we performed partial (90%) pancreatectomy (PX) or sham surgery in adult male rats (Figure 8A). Despite partial regeneration during the initial weeks of recovery, PX animals have sustained mild hyperglycemia and show selective loss of GSIS at 10 weeks after surgery (36, 37). As expected, PX rats had modest, but significantly elevated, fed blood glucose compared with sham animals (Figure 8B). Islets isolated 10 weeks after PX demonstrated decreased TE for highly expressed genes including *Ins1*, *Ins2*, *Scgn*, *Slc2a2*, and *Slc30a8* compared with sham with no effect on TE of *Tubg1* control (Figure 8C). For genes expressed at lower levels (*Vps41*, *Idh2*, *Pfkfb3*, and *Igf2*), recovery of mRNAs was insufficient to quantify TE. Steady-state protein levels were decreased for INS, SCGN, SLC2A2, and SLC30A8 (Figure 8D). Thus, sustained exposure to high glucose in a pathophysiologically relevant setting suppressed translation of key mRNAs required for metabolism-coupled insulin secretion and decreased abundance of their encoded proteins.

Discussion

In this study, we demonstrate that sustained high glucose selectively impairs mRNA translation of genes that serve critical roles at almost every step of glucose metabolism–coupled insulin secretion in pancreatic β cells. These nutrient-induced translation changes are coincident with impaired GSIS following prolonged exposure of cultured insulinoma cells or isolated islets ex vivo to high glucose and in the setting of 10 weeks of systemic hyperglycemia induced by partial pancreatectomy (PX). Our results show that programmatic dysregulation of β cell mRNA translation is a manifestation of glucose toxicity prior to the onset of ER stress or impairment of global translation. Translational downregulation decreases steady-state levels of these proteins, which serve important roles in GSIS and optimal β cell function.

β Cells leverage structural and functional specializations for coupling glucose metabolism to robust insulin peptide production and secretion. The insulin mRNA is highly abundant, and ER and Golgi are extensive in β cells (38, 39). Moreover, translation of insulin and genes involved in insulin processing and secretory granule biogenesis is rapidly and coordinately upregulated when glucose is acutely increased from basal to stimulatory concentrations (8, 9). Recently, high-throughput studies have shown that acute exposure of β cells to high glucose selectively upregulates translation of mRNAs encoding proteins related to insulin processing, exocytosis, and glucose metabolism, providing evidence that translation of functionally related proteins is coordinately regulated for optimal β cell function under physiological conditions (10, 11). Our findings establish that concerted β cell translational regulation occurs in the pathophysiological setting of chronic high glucose exposure. We show that sustained high glucose conditions that impair GSIS are associated with translational downregulation of mRNAs required for metabolism-coupled insulin secretion. Moreover, these translational changes result in decreased protein abundance, which likely contributes to decreased secretory function.

Consistent with prior reports (14, 19, 40), we found that exposure of rat and human islets to sustained high glucose decreased stimulation index but increased basal secretion. Although basal secretion and secretion following acute stimulation with glucose are supported by common components of the cellular machinery for secretion, regulation of these processes is distinct. Basal secretion is controlled by reactive oxygen species, redox regulation, and *S*-acylation–mediated trafficking (41), whereas GSIS is regulated by glucose metabolism, anaplerotic metabolism, the pentose monophosphate shunt, free fatty acids, the phosphoenolpyruvate cycle, and paracrine signals (42). These differences may underlie the divergent impacts of sustained high glucose on basal secretion (increased) and stimulation index (decreased). In both islets and MIN6 cells, sustained high glucose decreased stimulation index. Lack of increase in basal insulin secretion in the MIN6 β cell model may reflect the more modest capacity of these cells for insulin synthesis and the substantially decreased insulin content following exposure to sustained high glucose. In MIN6 cells and in islets, we used glucose concentrations previously demonstrated to impair
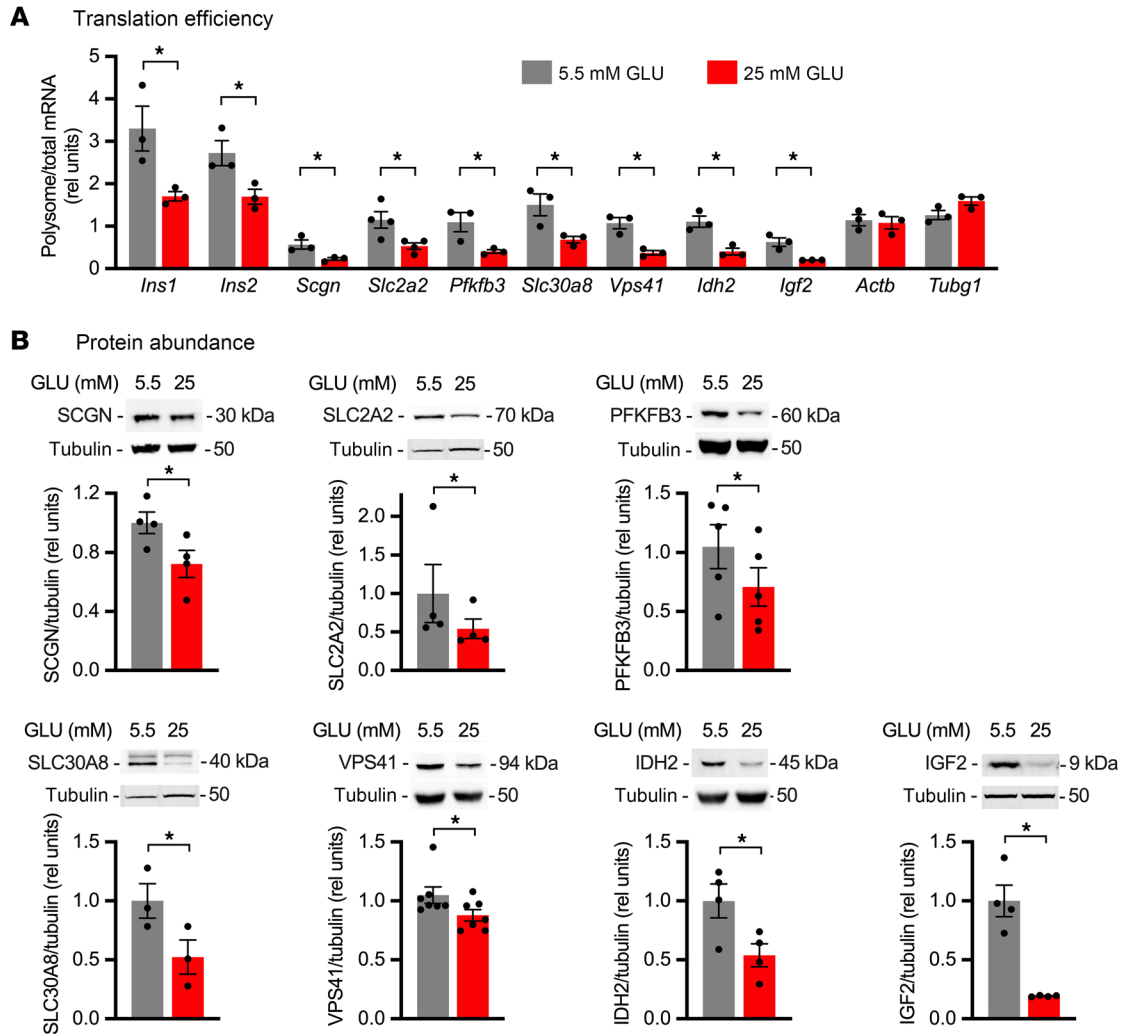
Figure 5. Translational regulation by sustained high glucose impacts protein abundance in MIN6 cells. MIN6 cells were incubated for 24 hours in medium containing 5.5 mM (gray) or 25 mM (red) GLU. (**A**) qPCR quantification of polysome and total RNA for *Ins1, Ins2, Scgn, Slc2a2, Pfkfb3, Slc30a8, Vps41, Idh2,* and *Igf2*, relative to 18S rRNA. *Actb* and *Tubg1* as controls. Mean ± SEM for *n* = 3–4 independent experiments. (**B**) Immunoblot of cell lysates for SCGN, SLC2A2, PFKFB3, SLC30A8, VPS41, IDH2, and IGF2. Tubulin loading control. Tubulin for the SLC2A2 panel and tubulin for the SLC30A8 panel are identical, since they were the same lanes on the gel. Representative blots with quantification of mean ± SEM for *n* = 3–7 independent experiments. *$P < 0.05$, unpaired *t* test (**A**) or ratio-paired *t* test (**B**).

GSIS (14, 16, 43). The different concentrations and durations of glucose needed to impair GSIS in insulinoma cells and islets from different species reflect intrinsic differences among these models.

β Cells synthesize up to a million proinsulin protein molecules per minute (44), creating a challenge for proper folding and processing of nascent proteins in the ER. Not surprisingly, prolonged exposure to high glucose can lead to ER stress that activates the unfolded protein response to decrease total mRNA translation (45). Our experimental design incorporated ex vivo treatment of islets and MIN6 cells with glucose at concentrations and for durations that did not increase ER stress markers in order to model early nutrient-induced changes. Consistent with the lack of engagement of the PERK-eIF2α arm of ER stress, total mRNA translation was unchanged under conditions in which we observed that translation of mRNAs involved in glucose-coupled insulin secretion was suppressed (46). It is also not surprising that ATF4 and JUND, proteins for which translation is increased under glucolipotox-

ic conditions that induce ER stress, were not upregulated in our study (17, 18). Our results indicate that programmatic alterations in translation of specific mRNAs occur prior to ER stress during the progression of β cell dysfunction.

Ribosome profiling has emerged as a powerful method for assessing mRNA translation in species ranging from yeast to human (47). However, TE calculated as the ratio of RPFs to RNA is an indirect measure of translation that could be confounded by translation pausing. Our strategy to also use nascent proteomics provided an approach to filter ribosome profiling results for translation changes that resulted specifically in synthesis of new proteins. As expected, only a fraction of newly synthesized proteins reflected altered TE, since nascent proteomics does not filter out changes resulting from increased mRNA abundance (48). We validated findings from MIN6 cell discovery studies in primary rat islets in which we demonstrated significant decreases in protein abundance for translationally downregulated genes. In the rat partial PX model,
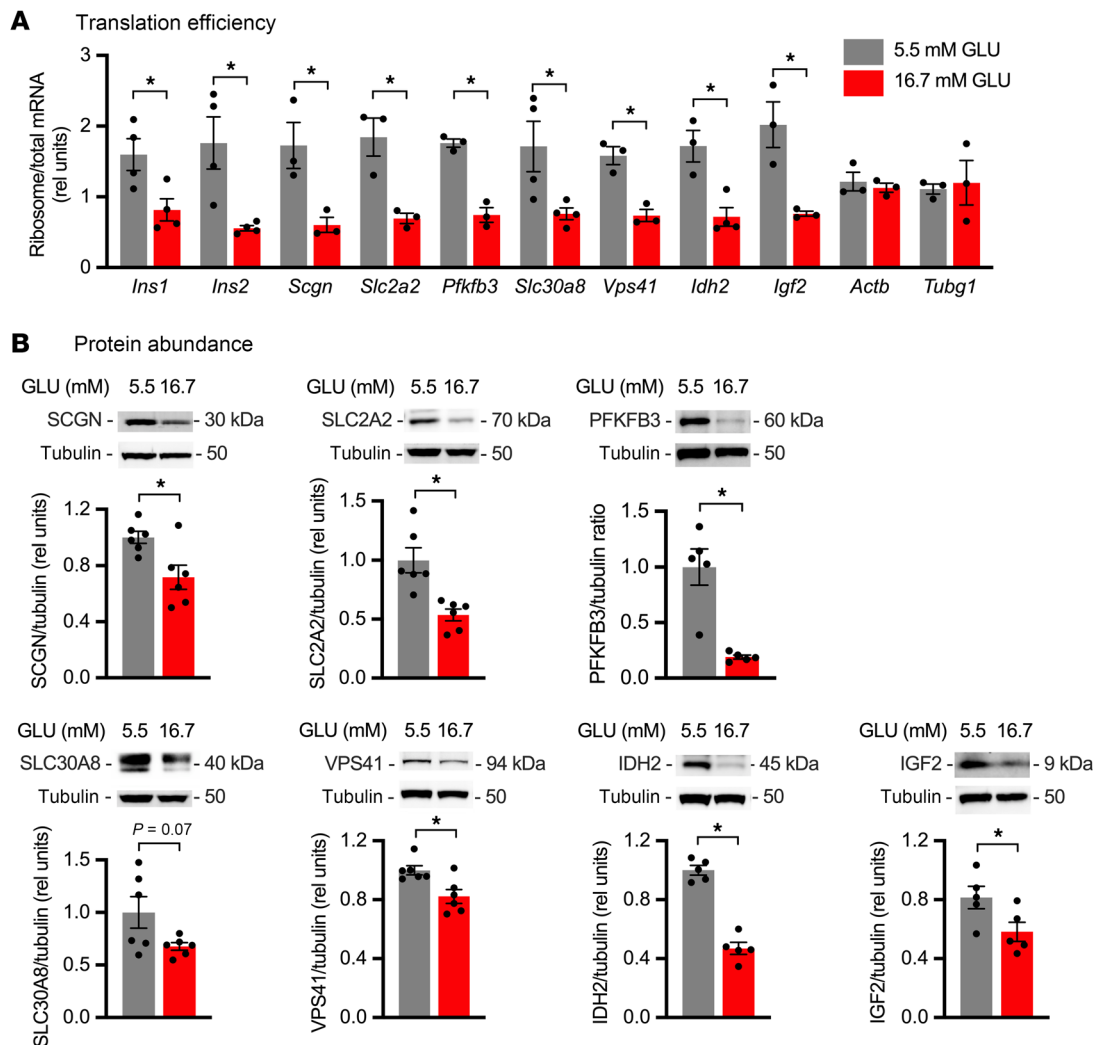
Figure 6. Translational regulation by sustained high glucose impacts protein abundance in rat islets. Primary rat islets were incubated for 4 days in medium containing 5.5 mM (gray) or 16.7 mM (red) GLU. (**A**) qPCR quantification of ribosome-associated and total RNA for *Ins1*, *Ins2*, *Scgn*, *Slc2a2*, *Pfkfb3*, *Slc30a8*, *Vps41*, *Idh2*, and *Igf2*, relative to 18S rRNA. *Actb* and *Tubg1* as controls. Mean ± SEM for n = 3–4 rats. (**B**) Representative immunoblots of islet lysates for SCGN, SLC2A2, PFKFB3, SLC30A8, VPS41, IDH2, and IGF2. Tubulin loading control. Tubulin for the SLC2A2 panel and tubulin for the SLC30A8 panel are identical, since they were the same lanes on the gel. Quantification of mean ± SEM for n = 5–6 rats. *P < 0.05, unpaired t test (**A**) or ratio-paired t test (**B**).

sustained mild hyperglycemia led to decreases in translation and protein abundance for the majority of these genes for which mRNA is highly abundant. Inability to quantify less abundant RNAs was likely a consequence of our experimental design to analyze islets immediately upon isolation without overnight recovery of the islets in order to capture the impact of in vivo glycemia. Nonetheless, the partial PX model provides important evidence that pathophysiological exposure to sustained high glucose over time produces similar dysregulation of islet mRNA translation as observed following ex vivo incubation of isolated islets.

Our human islet analyses largely phenocopied observations in rodent studies with several notable exceptions. First, TE for SLC2A1, but not SLC2A2, was significantly decreased in human islets, an observation that likely relates to species differences in glucose transporters (GLUT2/*Slc2a2* in rodent and GLUT1/*SLC2A1* in human β cells) (35). Second, absence of change

in *IDH2* and *IGF2* translation in human islets may reflect species differences in regulation of insulin secretion, as roles for these proteins in GSIS have been best characterized in rodents (31, 34). Overall, the magnitude of effect on mRNA translation in human islets was smaller than effects in MIN6 cells and rodent islets. This could relate to technical aspects of collection and handling of cadaveric tissue. Nonetheless, recapitulation of translational dysregulation by sustained high glucose in human islets supports the disease relevance of our findings.

mRNA-specific translational regulation is often driven by regulatory sequences that lie within the 5′- or 3′-UTRs of target RNAs and serve to increase or inhibit translation initiation (49). Neither Mfold (http://www.unafold.org/mfold/applications/rna-folding-form.php) nor RNAfold (http://rna.tbi.univie.ac.at/cgi-bin/RNAWebSuite/RNAfold.cgi), thermodynamic algorithms that maximize Watson-Crick base pairs and nearest-neighbor
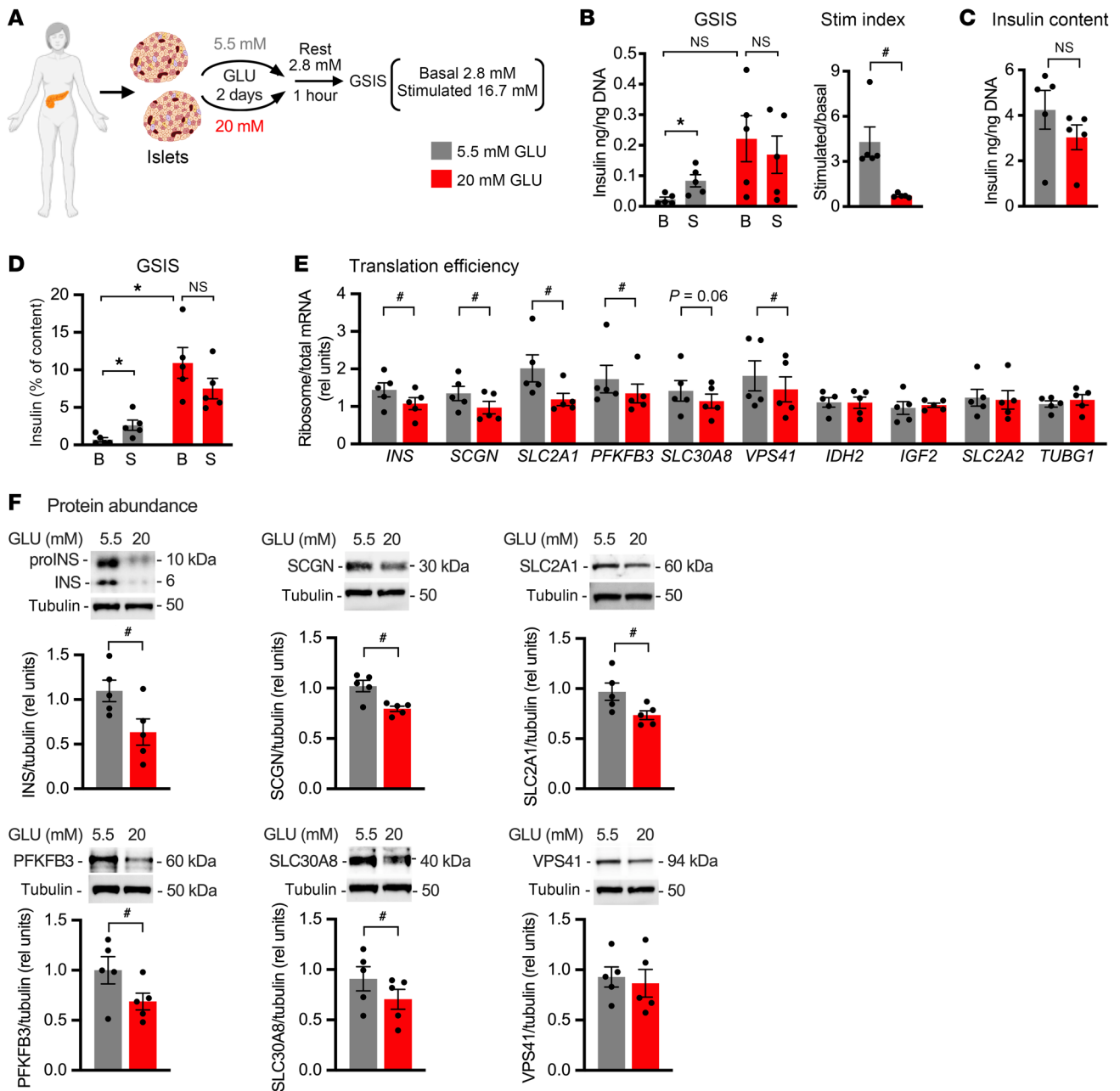
Figure 7. Translational regulation by sustained high glucose impacts protein abundance in human islets. Human cadaveric islets were cultured for 2 days in medium containing 5.5 mM (gray) or 20 mM (red) GLU. (**A**) One hour of resting in 2.8 mM GLU was followed by GSIS quantified at 2.8 mM (B) and 16.7 mM (S) GLU. (**B**) GSIS normalized by DNA with stimulation index quantified as stimulatory/basal secretion. (**C**) Insulin content normalized to DNA. (**D**) GSIS normalized to cellular insulin content. (**E**) qPCR quantification of ribosome-associated and total RNA for *INS*, *SCGN*, *SLC2A1*, *PFKFB3*, *SLC30A8*, *VPS41*, *IDH2*, *IGF2*, and *SLC2A2*, relative to 18S rRNA. *TUBG1* as control. (**F**) Representative immunoblots of islet lysates for INS, SCGN, SLC2A1, PFKFB3, SLC30A8, and VPS41. Tubulin as control. Tubulin for the SCGN panel and tubulin for the VPS41 panel are identical, since they were the same lanes on the gel. Quantification of mean ± SEM for $n = 5$ donors. *$P_{adj} < 0.05$, pre-planned paired t test (Bonferroni's post hoc correction, **B** [GSIS] and **D**). #$P < 0.05$, unpaired t test (**B** [Stim index] and **C**), paired t test (**E**), or ratio-paired t test (**F**).

parameters, predicted common secondary structural elements in the UTRs of the mRNAs that were translationally regulated by sustained high glucose. Moreover, we did not find common RNA-binding protein (RNAbp) motifs in the 5′- or 3′-UTRs of these mRNAs using the MEME Suite prediction algorithm (https://meme-suite.org/meme). Because in silico analyses of RNA primary sequence motifs and structure have limited sensitivity and specificity (50),

thorough evaluation of the contributions of UTRs to translational regulation of specific mRNAs by sustained high glucose will require in-depth experimental analyses that are beyond the scope of the present study.

Regulatory steps following transcription play an important role in determining gene expression, and simultaneous RNA sequencing and proteomic analyses combined with metabolic
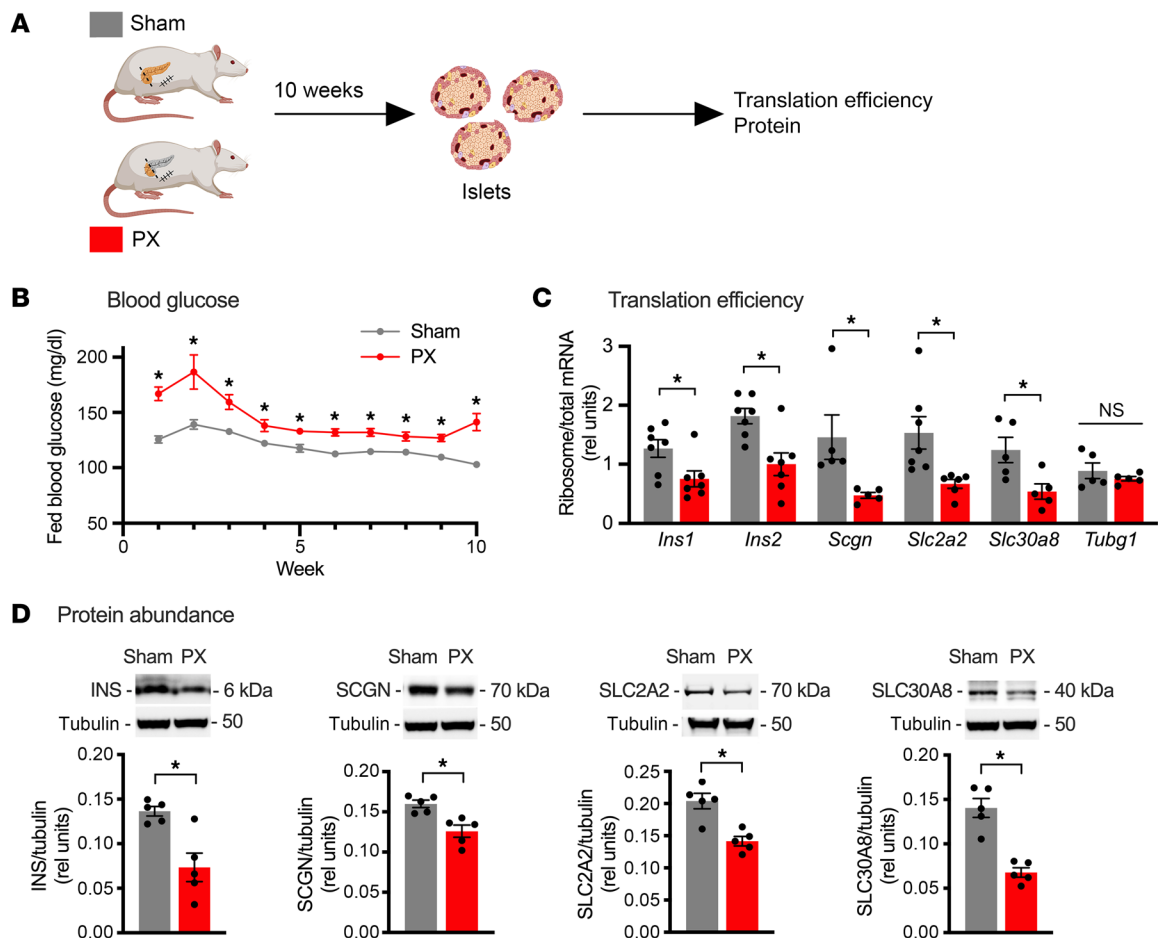
Figure 8. Translational regulation by hyperglycemia impacts protein abundance in partial pancreatectomy model of hyperglycemia. (**A**) Islets were isolated from Sprague-Dawley rats 10 weeks after sham (gray) or 90% pancreatectomy (PX, red) surgery. (**B**) Fed blood glucose. Mean ± SEM for n = 21 sham rats, n = 29 PX rats. (**C**) qPCR quantification of ribosome-associated and total islet RNA for *Ins1*, *Ins2*, *Scgn*, *Slc2a2*, and *Slc30a8*, relative to 18S rRNA. *Tubg1* as control. Mean ± SEM for n = 5–7 samples, each pooled from 2–3 rats. (**D**) Representative immunoblots of islet lysates for INS, SCGN, SLC2A2, and SLC30A8 with tubulin as control. Tubulin for INS panel, SCGN panel, and SLC30A8 panel is identical, since these were the same lanes on the gel. Quantification of mean ± SEM for n = 5 samples, each pooled from 2–3 rats. *P < 0.05, unpaired t test (**B**–**D**).

labeling of macromolecules provide evidence that mRNA-specific translation rates are a major determinant of the cellular proteome (51). Moreover, the development of high-throughput tools for discovery of coordinated mRNA-specific translation has advanced our understanding of how environmental cues shape gene expression. Our study provides insights into nutrient-driven translational regulation that alters the abundance of proteins important for insulin secretion in settings of β cell dysfunction. Future work to identify mechanisms by which glucose availability selectively and coordinately regulates translation of these mRNAs has the potential to identify novel strategies for interrupting β cell dysfunction early in the progression of diabetes.

Methods

Rodent islets. Islets were isolated from 7- to 8-week-old male Sprague-Dawley rats (Taconic Biosciences) by collagenase digestion followed by density gradient centrifugation as previously described (52). Islets were hand-picked and cultured overnight in RPMI 1640 containing 11 mM glucose, 10% FCS, 100 U/mL penicillin, 100 μg/mL streptomycin at 37°C with 5% CO_2. For analysis of GSIS, RNA, or protein, medium

was changed to RPMI medium containing either 5.5 mM or 16.7 mM glucose for 4 days.

Human islets. Islets from cadaveric nondiabetic donors (ages 30–50) (Supplemental Table 5) were obtained from Prodo Labs and cultured overnight in RPMI 1640 containing 5.5 mM glucose, 10% FCS, 100 U/ mL penicillin, 100 μg/mL streptomycin at 37°C with 5% CO_2. The following day, islets were incubated in medium containing either 5.5 mM or 20 mM glucose for 2 days before analysis of GSIS, RNA, or protein.

MIN6 cells. Low-passage MIN6 cells (provided by Jun-ichi Miyazaki) were cultured in DMEM containing 25 mM glucose, 15% FBS, 0.1 mM β-mercaptoethanol, 100 U/mL penicillin, and 100 μg/mL streptomycin at 37°C with 5% CO_2. For analyses of translation, MIN6 cells were incubated in DMEM containing 5.5 mM or 25 mM glucose for 24 hours before analysis of GSIS, RNA, or protein.

GSIS. Following incubations at different glucose concentrations, 10–12 islets (~150 μm diameter) in triplicate or MIN6 cells (10^5 per 35-mm well) in duplicate were washed and incubated with Krebs-Ringer bicarbonate HEPES buffer (KRBH: 137 mM NaCl, 4.8 mM KCl, 1.2 mM KH_2PO_4, 1.2 mM $MgSO_4 \cdot 7H_2O$, 2.5 mM $CaCl_2 \cdot 2H_2O$, 5 mM $NaHCO_3$, 16 mM HEPES, 0.1% BSA) containing 2.8 mM glucose

for 1 hour. After change of medium, cells were successively incubated in KRBH containing 2.8 and 16.7 (islet) or 16.8 mM (MIN6) glucose, each for 1 hour. Medium and cells were collected for insulin quantification by Ultra Sensitive Mouse Insulin ELISA (Crystal Chem; see Supplemental Table 7 for key reagents). Insulin was normalized to DNA content for islets (CyQuant cell proliferation kit, Fisher Scientific C7026) and to cell number for MIN6 cells.

mRNA quantitative reverse transcription PCR. Total RNA was isolated from cell lysates, sucrose density gradient fractions, or ribosome pellets using TRIzol or TRIzol LS reagents (Invitrogen) and Direct-zol RNA Miniprep kit (Zymo Research). RNA recovered from sucrose density gradient fractions was treated with 600 U/mL heparinase (NEB P0735S; 20 minutes, room temperature [RT]). Five hundred nanograms to 1 μg RNA was reverse-transcribed using iScript cDNA synthesis kit (Bio-Rad). Quantitative reverse transcription PCR was performed using SsoAdvanced Universal SYBR Green Supermix (Bio-Rad). RNA abundance was calculated according to the $\Delta\Delta Ct$ method relative to 18S rRNA. Primers are listed in Supplemental Table 6.

Quantification of nascent peptides using OPP. During the last 2 hours of incubations in different media, 20 μM O-propargyl-puromycin (OPP; Click Chemistry Tools) was added to the medium. Cells were lysed with RIPA buffer (50 mM Tris [pH 8], 150 mM NaCl, 0.5 % sodium deoxycholate, 1% NP-40, 0.1% SDS) containing cOmplete EDTA-free protease inhibitor cocktail (MilliporeSigma). Protein was quantified using bicinchoninic acid assay (Pierce). For in-gel quantification of total nascent peptides, 100–300 μg protein was used for copper-catalyzed cycloaddition reactions using the Click-iT Plus Alexa Fluor 647 Picolyl Azide Toolkit (Thermo Fisher Scientific). Proteins were separated using NuPAGE 10% Bis-Tris gels, and gels were fixed with 10% acetic acid, 50% methanol. Total nascent peptides were detected by in-gel imaging at 647 μm, and total protein was detected by Epi-far red imaging after staining with 0.1% Coomassie brilliant blue (Bio-Rad ChemiDoc MP Imaging System). For detection of nascent insulin and tubulin, 1 mg of cell lysate was used for cycloaddition reactions containing 5% SDS, 500 μM biotin azide, 5 mM DTT, 0.5 mM TBTA, and 5 mM $CuSO_4$ (1.5 hours, RT). Biotinylated protein was precipitated using methanol/chloroform, resuspended in RIPA buffer, and incubated overnight at 4°C with high-capacity streptavidin agarose beads (Pierce). Beads were washed twice sequentially with RIPA, 1 M KCl, 0.1 M Na_2CO_3, 2 M urea in 50 mM HEPES, RIPA again, and eluted with 2× Laemmli buffer. Proteins were separated using 10% NuPAGE Bis-Tris gels, and immunoblotting was used to detect nascent proteins. See Supplemental Table 7 for antibody sources and dilutions.

Immunoblotting. Islets were lysed by sonication in buffer containing 5 mM EDTA, 7 M urea, 2 M thiourea, 100 mM sodium fluoride, 100 mM pyrophosphate, 10 mM orthovanadate, 50 mM PMSF, 1 μg/mL aprotinin (Pierce 78432), and 1% Triton. MIN6 cells were lysed in RIPA buffer containing cOmplete protease inhibitor cocktail. Ten to twenty micrograms protein was separated on 10% NuPAGE Bis-Tris gels, transferred to PVDF membranes, blocked with 5% BSA, and blotted for the indicated proteins. Alexa Fluor–coupled (Invitrogen) secondary antibodies or HRP-coupled secondary antibodies (Cell Signaling Technology) and chemiluminescent substrates (Bio-Rad) were used for detection with a ChemiDoc MP Imaging System (Bio-Rad). For ER stress controls, islets were treated with 1 μM thapsigargin for 6 hours, and MIN6 cells were treated with 5 μg/mL tunicamycin for 3 hours. Antibodies and dilutions are listed in Supplemental Table 7.

Ribosome profiling. MIN6 cells incubated in medium with 5.5 mM or 25 mM glucose for 24 hours were treated with 100 μg/mL of cycloheximide for 5 minutes. Ribosome profiling was performed as previously described (53) except that 1 U/20 × 10^6 cells RNase 1 (Thermo Fisher Scientific) was used and rDNA depletion was performed using biotinylated rDNA sequences (47). Input RNA was extracted using TRIzol (Invitrogen) and Direct-zol RNA Miniprep kit. RNA libraries were generated using polyA enrichment and KAPA Stranded mRNA Hyper Prep (Illumina). RPF and RNA libraries were sequenced using Illumina NS500 single-end 75 bp reads. Data analyses used the XPRESSyourself pipeline (54). Briefly, trimmed reads were aligned to the genome (Ensembl release version 102) with the 2-pass option that removes rRNA alignments and PCR duplicates and counts reads that map to the exons or truncated coding sequences of the longest transcripts of protein-coding genes. XPRESSpipe was used for quality control analyses (RPF coverage, length, and periodicity) and to obtain normalized quantification of RNA, RPF counts, and TE defined as ratio of RPF to RNA. Differential expression and differential TE were performed using DESeq2 (55). Pathway analysis was performed by testing of overrepresentation of genes with differential TE in the Reactome gene sets from MSigDB using the pre-ranked CAMERA method in the limma package with the function cameraPR (56). Analysis of predicted structures of mRNA 5′- and 3′-untranslated regions was performed using Mfold and RNA-fold (57, 58). Analysis of untranslated regions for RNA binding protein motifs used MEME Suite (59).

Sucrose density gradient fractionation. Five percent to 50% sucrose gradients were generated using a BioComp Gradient Master IP from 5% and 50% sucrose solutions in sucrose buffer (10 mM Tris [pH 7.2], 60 mM KCl, 10 mM $MgCl_2$, 1 mM DTT, and 0.1 mg/mL heparin). MIN6 cells were treated with 100 μg/mL of cycloheximide for 5 minutes. Cells were lysed with ribosome profiling lysis buffer and layered onto gradients. After centrifugation (SW41T, Beckman Coulter; 222,200g, 3 hours, 4°C), fractions were collected using a BR-188 Density Gradient Fractionation System (Brandel). RNA was extracted from combined polysome fractions with TRIzol LS, and cleanup used Direct-zol RNA Miniprep kit.

Azidohomoalanine nascent proteomics. MIN6 cells were incubated in medium with 5.5 mM or 25 mM glucose for 24 hours. During the last 2.5 hours, cells were changed to methionine-free medium for 30 minutes, washed with PBS, and then incubated in methionine-free medium containing 250 μM azidohomoalanine (AHA) for 2 hours. Cells were collected and lysed in RIPA buffer containing cOmplete EDTA-free protease inhibitor cocktail, and proteins were quantified by bicinchoninic acid assay. Two milligrams protein per condition was reduced with 15 mM DTT (1 hour, RT), alkylated with 20 mM iodoacetamide (20 minutes, dark, RT), quenched with 10 mM DTT (15 minutes, dark, RT), precipitated using methanol/chloroform, and resuspended in 50 mM HEPES, 150 mM NaCl, 2% SDS (pH 7.2). Copper-catalyzed cycloaddition of biotin was performed with 1 mg of protein by addition of 100 μM TBTA, 1 mM sodium ascorbate, 1 mM copper sulfate, 100 μM biotin-alkyne (2 hours, RT). Proteins were precipitated to remove excess biotin-alkyne, resuspended in 2% SDS, 5 mM DTT, and diluted with RIPA buffer to a final SDS of less than 0.5%. Samples were mixed with 10 μL of high-capacity streptavidin beads (overnight, RT) and then washed twice sequentially with RIPA, 1 M KCl, 0.1 M Na_2CO_3, 2 M urea in 50 mM HEPES, RIPA again, and PBS (pH 7.4). Tryptic digest, TMT labeling, separation into 6 fractions, and LC-MS3 analysis were performed as previously described (60). MS2 spectra were searched using the Comet algorithm (61) against

a UniProt composite database derived from the mouse proteome, exogenous sequence, known contaminants, and reverse sequences. Peptide spectral matches were filtered to a 1% FDR using the target-decoy strategy combined with linear discriminant analysis. The proteins from the 6 runs were filtered to a <1% FDR. At least 2 unique peptides were required for identification, and proteins were quantified only from peptides with a summed SN threshold greater than 150. Protein intensity was $\log_2$ transformed, missing values were imputed, and data were normalized such that all samples had the same median abundance (62). We used limma to perform linear modeling and moderated t tests, with adjustment for surrogate variable analysis as previously described (63, 64).

Partial pancreatectomy. Six-week-old Sprague-Dawley (~100 g) male rats underwent 90% pancreatectomy or sham surgery as previously described (36). Under anesthesia with ketamine/xylazine, pancreatic tissue was removed by gentle abrasion with cotton-tipped applicators, leaving a small remnant 1–2 mm from the common bile duct and extending to the first loop of the duodenum. For sham surgery, the pancreas was disengaged from the mesentery but not removed. Postoperatively, body weights and morning fed glucose values were measured weekly. Ten weeks after surgery, islets were isolated as above and immediately lysed for analysis of total and ribosome-associated RNA and protein expression analysis.

Isolation of ribosome-associated mRNA from rat and human islets. After ex vivo incubation of rat and human islets with low or high glucose or immediately after isolation of islets from sham and PX rats, islets were treated with 100 µg/mL of cycloheximide for 5 minutes, washed with ice-cold PBS, and lysed with ribosome profiling buffer. One-third of the sample was collected for total RNA isolation, and the remaining material was centrifuged through a 1 M sucrose cushion to collect pelleted ribosome-associated mRNA (435,400g, 1 hour, 4°C). Total and ribosome-associated mRNA was isolated using TRIzol (Invitrogen) and 1-bromo-3-chloropropane (MilliporeSigma) by phase separation method.

Statistics. For biochemical, cell biological, and physiological experiments, analyses were performed using GraphPad Prism. Data are presented as mean ± SEM. Statistical significance was determined by unpaired or paired 2-tailed t tests, as described in figure legends, and P values less than 0.05 were considered significant. For multiple comparisons, 2-way ANOVA or 2-tailed t tests followed by Bonferroni's correction were performed, and adjusted P values less than 0.05 were considered significant. For ribosome profiling and nascent proteomics, P values were adjusted for multiple tests and FDR < 0.1 (Benjamini-Hochberg method) was considered significant. Figures were generated using GraphPad Prism and BioRender.com.

Study approval. All procedures using animals were approved by the Joslin Diabetes Center Institutional Animal Care and Use Committee. The Joslin Diabetes Center Committee on Human Studies determined that studies of deidentified cadaveric human islets do not constitute human subject research.

Data availability. RNA sequencing data are available from the NCBI's Gene Expression Omnibus (GEO) database (accession GSE248349). Proteomics data are available on PRoteomics IDEntifications database (PRIDE) (accession PXD047140). The Supporting Data Values file will be made available by the corresponding author upon request.

1. Halban PA, et al. β-cell failure in type 2 diabetes: postulated mechanisms and prospects for prevention and treatment. *Diabetes Care*. 2014;37(6):1751–1758.
2. Evans-Molina C, et al. β Cell dysfunction exists more than 5 years before type 1 diabetes diagnosis. *JCI Insight*. 2018;3(15):e120877.
3. [No authors listed]. Effect of intensive therapy on residual beta-cell function in patients with type 1 diabetes in the Diabetes Control and Complications trial. A randomized, controlled trial. The Diabetes Control and Complications Trial Research Group. *Ann Intern Med*. 1998;128(7):517–523.
4. Chen HS, et al. Beneficial effects of insulin on glycemic control and beta-cell function in newly diagnosed type 2 diabetes with severe hyperglycemia after short-term intensive insulin therapy. *Diabetes Care*. 2008;31(10):1927–1932.
5. Garvey WT, et al. The effect of insulin treatment on insulin secretion and insulin action in type II diabetes mellitus. *Diabetes*. 1985;34(3):222–234.
6. Itoh N, Okamoto H. Translational control of proinsulin synthesis by glucose. *Nature*. 1980;283(5742):100–102.
7. Wicksteed B, et al. A cis-element in the 5′ untranslated region of the preproinsulin mRNA (ppIGE) is required for glucose regulation of proinsulin translation. *Cell Metab*. 2007;5(3):221–227.
8. Guest PC, et al. Insulin secretory granule biogenesis. Co-ordinate regulation of the biosynthesis of the majority of constituent proteins. *Biochem J*. 1991;274(pt 1):73–78.
9. Alarcon C, et al. The biosynthesis of the subtilisin-related proprotein convertase PC3, but no that of the PC2 convertase, is regulated by glucose in parallel to proinsulin biosynthesis in rat pancreatic islets. *J Biol Chem*. 1993;268(6):4276–4280.
10. Zakaria A, et al. Glucose treatment of human pancreatic β-cells enhances translation of mRNAs involved in energetics and insulin secretion. *J Biol Chem*. 2021;297(1):100839.
11. Bulfoni M, et al. Glucose controls co-translation of structurally related mRNAs *via* the mTOR and eIF2 pathways in human pancreatic beta cells. *Front Endocrinol (Lausanne)*. 2022;13:949097.
12. Schatz H, et al. (Pro-) insulin biosynthesis and release of newly synthesized (pro-) insulin from isolated islets of rat pancreas in the presence of amino acids and sulphonylureas. *Eur J Clin Invest*. 1975;5(6):477–485.
13. Mittendorfer B, et al. β Cell function and plasma insulin clearance in people with obesity and different glycemic status. *J Clin Invest*. 2022;132(3):e154068.
14. Eizirik DL, et al. Prolonged exposure of human pancreatic islets to high glucose concentrations in vitro impairs the beta-cell function. *J Clin Invest*. 1992;90(4):1263–1268.
15. Ling Z, et al. Effects of chronically elevated

glucose levels on the functional properties of rat pancreatic beta-cells. *Diabetes*. 1996;45(12):1774–1782.

16. Marselli L, et al. Persistent or transient human β cell dysfunction induced by metabolic stress: specific signatures and shared gene expression with type 2 diabetes. *Cell Rep*. 2020;33(9):108466.

17. Good AL, et al. JUND regulates pancreatic β cell survival during metabolic stress. *Mol Metab*. 2019;25:95–106.

18. Hatanaka M, et al. Palmitate induces mRNA translation and increases ER protein load in islet β-cells via activation of the mammalian target of rapamycin pathway. *Diabetes*. 2014;63(10):3404–3415.

19. Kaiser N, et al. Monolayer culture of adult rat pancreatic islets on extracellular matrix: modulation of B-cell function by chronic exposure to high glucose. *Endocrinology*. 1991;129(4):2067–2076.

20. Cnop M, et al. Endoplasmic reticulum stress and eIF2α phosphorylation: the Achilles heel of pancreatic β cells. *Mol Metab*. 2017;6(9):1024–1039.

21. Shrestha N, et al. Pathological β-cell endoplasmic reticulum stress in type 2 diabetes: current evidence. *Front Endocrinol (Lausanne)*. 2021;12:650158.

22. Miyazaki J, et al. Establishment of a pancreatic beta cell line that retains glucose-inducible insulin secretion: special reference to expression of glucose transporter isoforms. *Endocrinology*. 1990;127(1):126–132.

23. Guo H, et al. Mammalian microRNAs predominantly act to decrease target mRNA levels. *Nature*. 2010;466(7308):835–840.

24. Pullen TJ, et al. Analysis of purified pancreatic islet beta and alpha cell transcriptomes reveals 11β-hydroxysteroid dehydrogenase (Hsd11b1) as a novel disallowed gene. *Front Genet*. 2017;8:41.

25. Yang SY, et al. Secretagogin affects insulin secretion in pancreatic β-cells by regulating actin dynamics and focal adhesion. *Biochem J*. 2016;473(12):1791–1803.

26. Kobayashi M, et al. Functional analysis of novel candidate regulators of insulin secretion in the min6 mouse pancreatic β cell line. *PLoS One*. 2016;11(3):e0151927.

27. Hasegawa K, et al. The hydrolase DDAH2 enhances pancreatic insulin secretion by transcriptional regulation of secretagogin through a Sirt1-dependent mechanism in mice. *FASEB J*. 2013;27(6):2301–2315.

28. Wijesekara N, et al. Beta cell-specific Znt8 deletion in mice causes marked defects in insulin processing, crystallisation and secretion. *Diabetologia*. 2010;53(8):1656–1668.

29. Burns CH, et al. Pancreatic β-cell-specific deletion of VPS41 causes diabetes due to defects in insulin secretion. *Diabetes*. 2021;70(2):436–448.

30. Low BSJ, et al. Decreased GLUT2 and glucose uptake contribute to insulin secretion defects in MODY3/HNF1A hiPSC-derived mutant β cells. *Nat Commun*. 2021;12(1):3133.

31. Zhang GF, et al. Reductive TCA cycle metabolism fuels glutamine- and glucose-stimulated insulin secretion. *Cell Metab*. 2021;33(4):804–817.

32. Guillam MT, et al. Early diabetes and abnormal postnatal pancreatic islet development in mice lacking Glut-2. *Nat Genet*. 1997;17(3):327–330.

33. Arden C, et al. A role for PFK-2/FBPase-2, as distinct from fructose 2,6-bisphosphate, in regulation of insulin secretion in pancreatic beta-cells. *Biochem J*. 2008;411(1):41–51.

34. Modi H, et al. Autocrine action of IGF2 regulates adult beta-cell mass and function. *Diabetes*. 2015;64(12):4148–4157.

35. De Vos A, et al. Human and rat beta cells differ in glucose transporter but not in glucokinase gene expression. *J Clin Invest*. 1995;96(5):2489–2495.

36. Bonner-Weir S, et al. Partial pancreatectomy in the rat and subsequent defect in glucose-induced insulin release. *J Clin Invest*. 1983;71(6):1544–1553.

37. Leahy JL, et al. Minimal chronic hyperglycemia is a critical determinant of impaired insulin secretion after an incomplete pancreatectomy. *J Clin Invest*. 1988;81(5):1407–1414.

38. Tillmar L, et al. Control of insulin mRNA stability in rat pancreatic islets. Regulatory role of a 3′-untranslated region pyrimidine-rich sequence. *J Biol Chem*. 2002;277(2):1099–1106.

39. Dean PM. Ultrastructural morphometry of the pancreatic β-cell. *Diabetologia*. 1973;9(2):115–119.

40. Purrello F, et al. Effects of high glucose on insulin secretion by isolated rat islets and purified beta-cells and possible role of glycosylation. *Diabetes*. 1989;38(11):1417–1422.

41. Corkey BE, et al. What regulates basal insulin secretion and causes hyperinsulinemia? *Diabetes*. 2021;70(10):2174–2182.

42. Campbell JE, Newgard CB. Mechanisms controlling pancreatic islet cell function in insulin secretion. *Nat Rev Mol Cell Biol*. 2021;22(2):142–158.

43. Zhang Z, et al. High glucose inhibits glucose-6-phosphate dehydrogenase, leading to increased oxidative stress and beta-cell apoptosis. *FASEB J*. 2010;24(5):1497–1505.

44. Schuit FC, et al. Glucose stimulates proinsulin biosynthesis by a dose-dependent recruitment of pancreatic beta cells. *Proc Natl Acad Sci U S A*. 1988;85(11):3865–3869.

45. Laybutt DR, et al. Endoplasmic reticulum stress contributes to beta cell apoptosis in type 2 diabetes. *Diabetologia*. 2007;50(4):752–763.

46. Shi Y, et al. Identification and characterization of pancreatic eukaryotic initiation factor 2 alpha-subunit kinase, PEK, involved in translational control. *Mol Cell Biol*. 1998;18(12):7499–7509.

47. Ingolia NT, et al. The ribosome profiling strategy for monitoring translation in vivo by deep sequencing of ribosome-protected mRNA fragments. *Nat Protoc*. 2012;7(8):1534–1550.

48. Dieterich DC, et al. Labeling, detection and identification of newly synthesized proteomes with bioorthogonal non-canonical amino-acid tagging. *Nat Protoc*. 2007;2(3):532–540.

49. Gebauer F, Hentze MW. Molecular mechanisms of translational control. *Nat Rev Mol Cell Biol*. 2004;5(10):827–835.

50. Vicens Q, Kieft JS. Thoughts on how to think (and talk) about RNA structure. *Proc Natl Acad Sci U S A*. 2022;119(17):e2112677119.

51. Schwanhausser B, et al. Global quantification of mammalian gene expression control. *Nature*. 2011;473(7347):337–342.

52. Gotoh M, et al. Reproducible high yield of rat islets by stationary in vitro digestion following pancreatic ductal or portal venous collagenase injection. *Transplantation*. 1987;43(5):725–730.

53. McGlincy NJ, Ingolia NT. Transcriptome-wide measurement of translation by ribosome profiling. *Methods*. 2017;126:112–129.

54. Berg JA, et al. XPRESSyourself: enhancing, standardizing, and automating ribosome profiling computational analyses yields improved insight into data. *PLoS Comput Biol*. 2020;16(1):e1007625.

55. Love MI, et al. Moderated estimation of fold change and dispersion for RNA-seq data with DESeq2. *Genome Biol*. 2014;15(12):550.

56. Wu D, Smyth GK. Camera: a competitive gene set test accounting for inter-gene correlation. *Nucleic Acids Res*. 2012;40(17):e133.

57. Gruber AR, et al. The Vienna RNA websuite. *Nucleic Acids Res*. 2008;36(web server issue):W70–W74.

58. Zuker M. Mfold web server for nucleic acid folding and hybridization prediction. *Nucleic Acids Res*. 2003;31(13):3406–3415.

59. Bailey TL, et al. The MEME Suite. *Nucleic Acids Res*. 2015;43(w1):W39–W49.

60. An H, et al. Systematic quantitative analysis of ribosome inventory during nutrient stress. *Nature*. 2020;583(7815):303–309.

61. Eng JK, et al. Comet: an open-source MS/MS sequence database search tool. *Proteomics*. 2013;13(1):22–24.

62. Stekhoven DJ, Buhlmann P. MissForest—non-parametric missing value imputation for mixed-type data. *Bioinformatics*. 2012;28(1):112–118.

63. Leek JT, Storey JD. Capturing heterogeneity in gene expression studies by surrogate variable analysis. *PLoS Genet*. 2007;3(9):1724–1735.

64. Ritchie ME, et al. limma powers differential expression analyses for RNA-sequencing and microarray studies. *Nucleic Acids Res*. 2015;43(7):e47.